

Examining long-term variability in saturated hydraulic conductivity of sandy soils and its influencing factors

Saeed Nikghalb Ashouri¹, Adrian Pittari¹, Vicki Moon¹, and Ali Shokri¹

¹Waikato University

September 13, 2023

Abstract

Saturated hydraulic conductivity (Ks) is a crucial parameter that influences water flow in saturated soils, with applications in various fields such as surface water runoff, soil erosion, drainage, and solute transport. However, accurate estimation of Ks is challenging due to temporal and spatial uncertainties. This study addresses the knowledge gap regarding the long-term behaviour of Ks in sandy soils with less than 10% fine particles. The research investigates the changes in Ks over a long period of constant head tests and examines the factors influencing its variation. Two sandy samples were tested using a hydraulic conductivity cell, and the hydraulic head and discharge were recorded for over 50 days. The results show a general decline in Ks throughout the test, except for brief periods of increase. Furthermore, the relationship between flow rate and hydraulic head gradient does not follow the expected linear correlation from Darcy's law, highlighting the complex nature of sandy soil hydraulic conductivity. The investigation of soil properties in three different sections of the samples before and after the tests revealed a decrease in the percentage of fine particles and a shift in specific gravity from the bottom to the top of the sample, suggesting particle migration along the flow direction. Factors such as clogging by fine particles and pore pressure variation contribute to the changes in Ks. The implications of this study have far-reaching effects on various geotechnical engineering applications. These include groundwater remediation, geotechnical stability analysis, and drainage system design.

Hosted file

972606_0_art_file_11334405_s0js72.docx available at <https://authorea.com/users/664099/articles/665992-examining-long-term-variability-in-saturated-hydraulic-conductivity-of-sandy-soils-and-its-influencing-factors>

Examining long-term variability in saturated hydraulic conductivity of sandy soils and its influencing factors

Saeed Nikghalb Ashouri¹, Adrian Pittari¹, Vicki Moon¹, Ali Shokri¹

1. Waikato University, New Zealand

Abstract

Saturated hydraulic conductivity (K_s) is a crucial parameter that influences water flow in saturated soils, with applications in various fields such as surface water runoff, soil erosion, drainage, and solute transport. However, accurate estimation of K_s is challenging due to temporal and spatial uncertainties. This study addresses the knowledge gap regarding the long-term behaviour of K_s in sandy soils with less than 10% fine particles. The research investigates the changes in K_s over a long period of constant head tests and examines the factors influencing its variation. Two sandy samples were tested using a hydraulic conductivity cell, and the hydraulic head and discharge were recorded for over 50 days. The results show a general decline in K_s throughout the test, except for brief periods of increase. Furthermore, the relationship between flow rate and hydraulic head gradient does not follow the expected linear correlation from Darcy's law, highlighting the complex nature of sandy soil hydraulic conductivity. The investigation of soil properties in three different sections of the samples before and after the tests revealed a decrease in the percentage of fine particles and a shift in specific gravity from the bottom to the top of the sample, suggesting particle migration along the flow direction. Factors such as clogging by fine particles and pore pressure variation contribute to the changes in K_s . The implications of this study have far-reaching effects on various geotechnical engineering applications. These include groundwater remediation, geotechnical stability analysis, and drainage system design.

Keywords: Saturated hydraulic conductivity, constant head test, clogging, sandy soil, drainable pores

1. Introduction

The saturated hydraulic conductivity (K_s) plays a crucial role in determining the water flow rate within the saturated zone of soils. This parameter is essential in various fields of study, including surface water runoff, soil erosion, deep percolation, drainage, crop simulation models, and solute transport (Ben-Hur et al., 2009; Boadu, 2000; Hwang et al., 2017; Suleiman & Ritchie, 2001). Using

31 the Darcy equation, K_s can be defined as the ratio of water flow (Q) in the unit section of saturated
32 soil (A) to the hydraulic gradient (i). The parameter K_s is present in the majority of equations
33 related to water flow in a saturated medium, yet its estimation can be challenging both in the
34 laboratory and the field due to temporal and spatial uncertainties (Suleiman & Ritchie, 2001).

35 Laboratory estimations of K_s utilise three standard methods: constant head, falling head, and
36 constant flow rate, as detailed in ASTM D5856-15 (2015). When dealing with granular and
37 disturbed samples containing less than 10% of fine particles passing 75 μm or No. 200 sieve, the
38 recommended approach is the constant head method, as outlined in ASTM D2434-19 (2019).
39 Conversely, samples comprising more than 10% of fine particles can be analysed using any of the
40 three mentioned methods. However, K_s measurements are conducted using a rigid-wall,
41 compaction-mold permeameter, with specific criteria provided in ASTM D5856 (2015).

42 Extensive research has been conducted on the long-term variations of hydraulic conductivity in
43 low-permeability soils, which are commonly employed in landfill sites and artificial wetlands. From
44 the perspective of an Earth scientist, these materials might be perceived as loose sediment or
45 deposits rather than the conventional 'soil,' which typically encompasses a mixture of inorganic and
46 organic constituents. In landfills, leachate, and artificial wetlands, contaminated water from roads
47 needs to be contained to gradually remove the pollutants from the water and prevent pollution of
48 underground water resources (Fang et al., 2022; Li et al., 2023; Shaver, 2020; Touze-Foltz et al.,
49 2006; Valencia-González et al., 2022; W. Wang et al., 2023). Therefore, the application of a layer
50 with very low permeability is necessary to reduce the infiltration of contaminated water into the
51 soil while simultaneously eliminating pollutants. Several studies have shown that the K_s in low
52 permeability soil samples change with infiltration of the water that contains chemical or biological
53 agents (Francisca & Glatstein, 2010; Liu & Liu, 2020; Lu et al., 2020; Montoro & Francisca, 2010).

54 Chemical substances present in the fluid can create a chemical imbalance and interfere with ion
55 exchange processes in the soil, leading to fluctuations in K_s . According to a study conducted by Jo et
56 al. (2005), a 3-year test observed a tenfold variation in K_s of a clay liner permeated by leachate-
57 containing chemical agents. In their tests, the hydraulic conductivity of one of the samples reached
58 stability after about 1.5 years of the test. On the other hand, the formation of microorganisms and
59 the presence of nutrients to feed them can cause clogging in the soil and, hence, a reduction in the
60 drainable pores and K_s (Fang et al., 2022; VanGulck & Rowe, 2004).

61 In sandy soils, the duration of the test is usually relatively short. It is commonly assumed that the
62 test can be concluded when four samples yield values within $\pm 25\%$ of the mean calculated from

63 these four samples throughout the test (ASTM D5856-15, 2015). Also, there is no reference to the
64 length of the test in ASTM D2434-19 (2019). However, several studies suggest that the hydraulic
65 conductivity of sandy soils can change over time. For example, there has been extensive research on
66 the variation of hydraulic conductivity in groundwater artificial recharge (Konikow et al., 2001;
67 Mays & Hunt, 2005; Siriwardene et al., 2007; Song et al., 2020; Ye et al., 2019). Vanderzalm et al.
68 (2020) and Du et al. (2018) subjected sandy samples to water permeation containing suspended
69 solids and *Fe (III)* ions, respectively, for an extended period (40 days in the former case and seven
70 days in the latter study), leading to observed fluctuations in *K_s* that demonstrate a prevalent
71 declining pattern over time. These studies identified physical and biological clogging mechanisms
72 as dominant factors for *K_s* variation. However, neither of the above studies has tested a sample
73 permeated with distilled water or tap water with minimum suspended solids or chemicals to
74 ensure that *K_s* remains constant under minimum influent contamination. Du et al. (2013) and Z.
75 Wang Et al. (2012) used tap water with and without suspended solids in a constant head test on
76 quartz sand samples and observed a noticeable drop in *K_s* over four days. Siriwardene et al. (2007)
77 also reported a reduction in the *K_s* when the sample was permeated with tap water containing
78 suspended solids. They noticed clogging of the suspended solids in the lower section of the sample
79 as the main reason for the noticeable drop in the *K_s*, whereas Z. Wang et al. (2012) showed that
80 finer suspended solids could travel deeper in the sample and cause blockage of the drainable pores.

81 Clogging can also be caused by the internal mobilisation or swelling of fine particles in the soil
82 (Jeong et al., 2018a; Konikow et al., 2001; Mohan et al., 1993; Torkzaban et al., 2015). Additionally,
83 clay minerals like *Illite*, *Kaolinite*, and *Montmorillonite* can be washed with water, leading to the
84 blockage of drainable pores in the sample and a reduction in *K_s* (Cihan et al., 2022; Jeong et al.,
85 2018a; Y. Wang et al., 2021). Stormwater management devices like artificial soakage basins and
86 soak pits are commonly recommended in new urban developments with high infiltration rates
87 (Shaver, 2020). Furthermore, with the widespread use of artificial groundwater recharge, the long-
88 term behaviour of *K_s* in sandy materials gains significant importance. Variations in *K_s* and pore
89 blockages can profoundly influence the effectiveness of design strategies employed in stormwater
90 management and groundwater recharge scenarios.

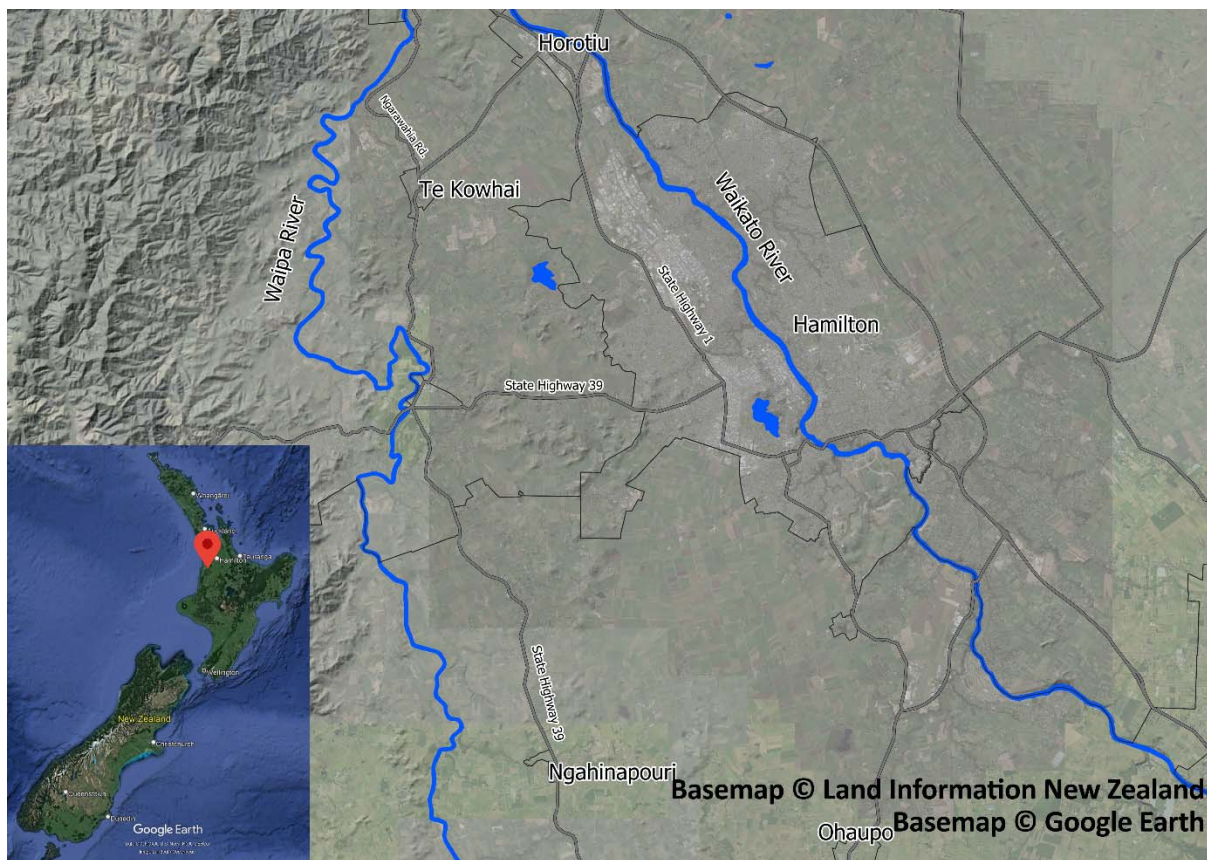
91 Currently, there is a lack of research focusing on the extended-duration variations in *K_s* within
92 sandy soils due to fluctuating hydraulic levels. Observing *K_s* over the long term provides insights
93 into the sustained groundwater movement within the aquifer, with changes in hydraulic levels
94 indicating shifts in aquifer water levels during and after rainfall events. This study aims to bridge
95 the knowledge gap regarding the prolonged behaviour of hydraulic conductivity in sandy soils.

96 Although various research has explored short-term K_s variations, particularly in the context of
97 stormwater management devices, a comprehensive understanding of how K_s evolves over extended
98 timeframes remains limited. Grasping the long-term behaviour of K_s holds critical significance for
99 the effectiveness of soakage systems and safeguarding subsurface water resources. Thus, this paper
100 illuminates the key factors shaping K_s variations over prolonged periods.

101 2. Materials

102 2.1. Sample source and physical properties

103 The soil examined in this study is river sand, commercially referred to as pit sand, often employed
104 for embankments and raised areas like pathways. The pit sand used for this investigation
105 originated from sand quarries situated in Ngahinapouri and Te Kowhai, located along the Waipa
106 River in Waikato, New Zealand, as depicted in Figure 1. For this study, two samples (sample *A* and
107 sample *B*) were taken from the same batch of pit sand provided by a supplier. Sample *B* was used as
108 a replication in this research.



109

110 *Figure 1- The geographical location of the Waipa River in New Zealand, with the samples originating*
111 *from sand quarries located near the Waipa riverbanks.*

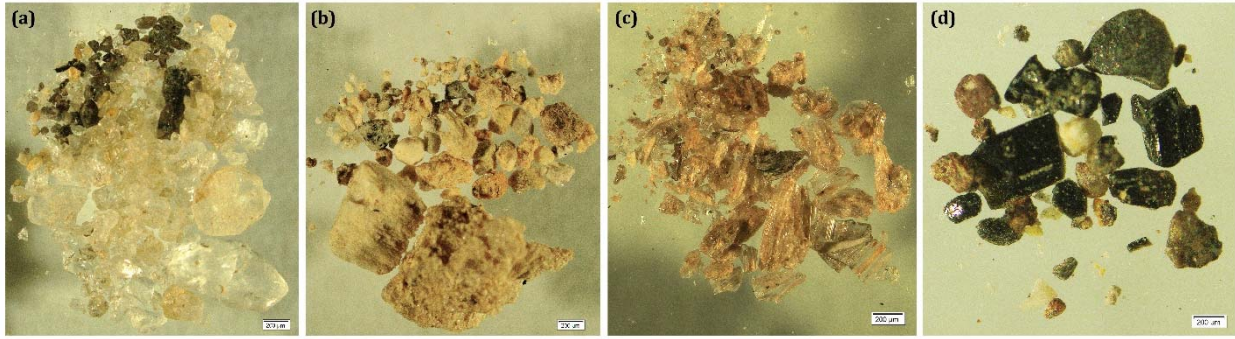
112 Table 1 outlines the physical properties of the samples. Upon microscopic examination and particle
 113 separation, five distinct groups are discerned (Figure 2): quartz and feldspar (approximately 60%),
 114 pumice (approximately 11%), colourful particles (approximately 6%), magnetics (approximately
 115 10%), and glass shards (approximately 13%). The magnetic minerals were isolated through
 116 magnetic separation. X-ray diffraction (XRD) analysis was employed to assess mineral composition,
 117 while the loss on ignition (LOI) method was utilised to estimate the presence of organic material in
 118 the samples. The analysis of XRD data peak patterns confirms that quartz and feldspar constitute
 119 the majority of minerals in the sample (Figure 3).

120 A laser diffractometer (Malvern Mastersizer 3000) was used to determine the particle size
 121 distribution of the samples. For this study, the particles below $75 \mu m$ were considered as fines,
 122 which aligns with the classification of ASTM for fine and coarse particles (ASTM D2487, 2020). The
 123 particle size distribution results indicate that the samples are primarily sandy, with less than 10%
 124 of fine materials. Particles below $5 \mu m$ were considered mobile colloidal particles (Kretzschmar et
 125 al., 1999), and the percentages of these particles are also mentioned in Table 1. Based on Standard
 126 Proctor tests (ASTM, 2012), the optimal compaction moisture of the samples was determined to be
 127 12%.

128 *Table 1- Properties of tested samples*

Parameter	Sample A	Sample B
Specific gravity of grains	2.6739	-
Specific surface (m ² /kg)	84.60	102.90
Particles < 5 μm (%)	2.3	2.6
Particles 5-75 μm (%)	5.06	5.83
Particles > 75 μm (%)	92.61	91.56
Dry density (g/cm ³)	1.289	1.261
Optimal gravimetric compaction moisture (%)	12	12
Sample gravimetric moisture (%)*	8.1	11.8
Organic matter	1.7%	1.7%

129 * Sample gravimetric moisture was measured when the sample was compacted in the mould. A
 130 small amount of sample A and B was taken and dried in the oven, and moisture was measured.

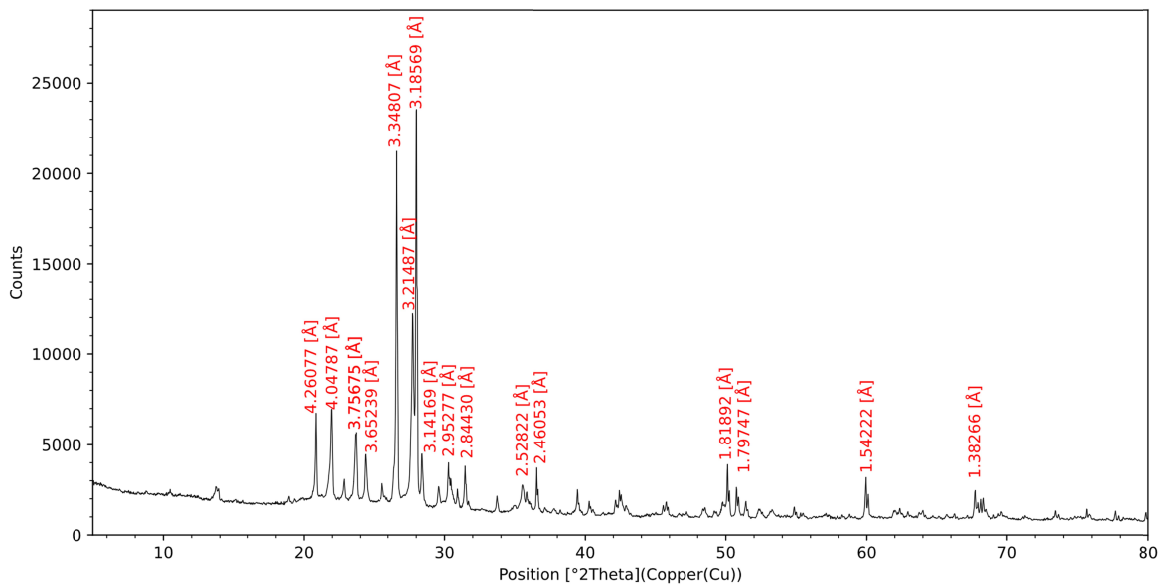


131

132

133

Figure 2- Separation of particles under microscope: (a) Quartz and feldspar, (b) Pumice, (c), glass shards, and (d) colourful minerals



134

135

136

Figure 3- XRD analysis of the sample: Major peaks are related to the quartz and feldspar content in the sample

137 2.2. Sample preparation

138

139

140

141

142

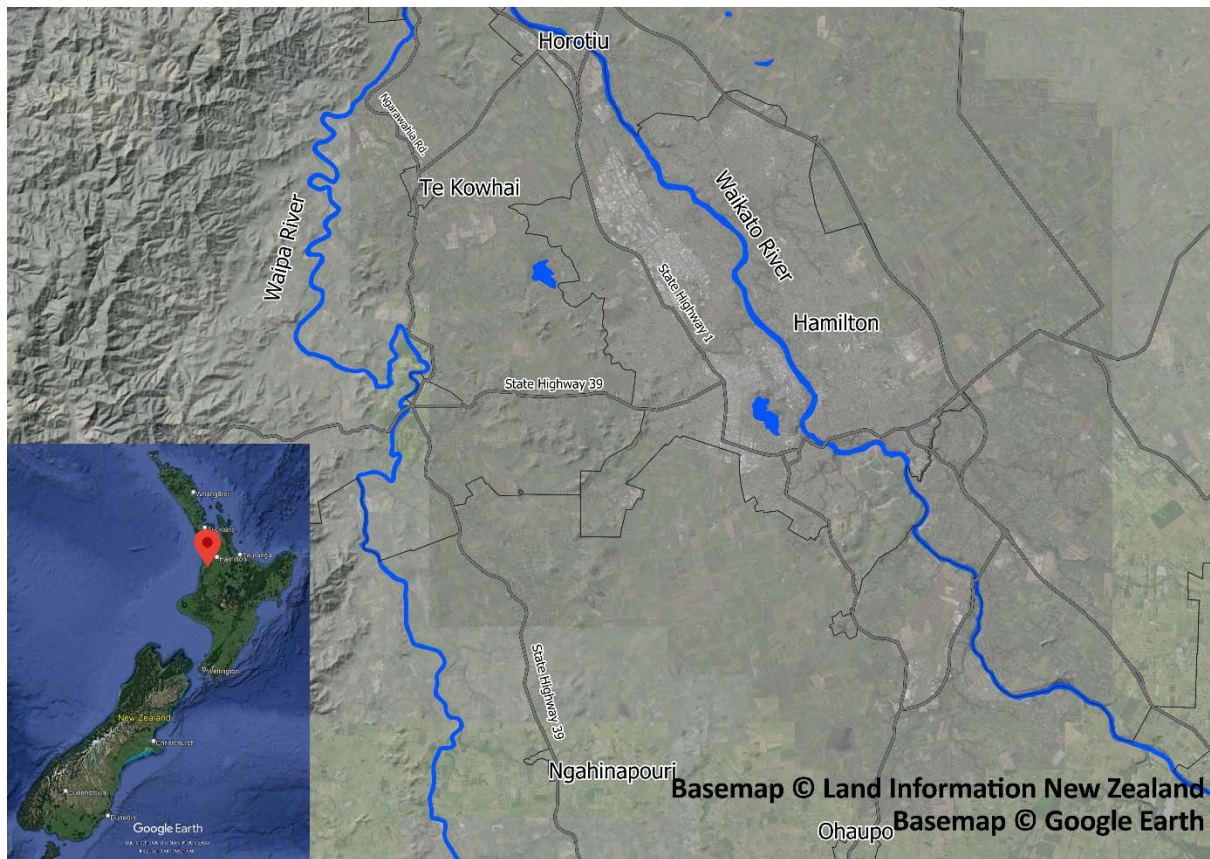
143

144

145

Prior to conducting the tests, the samples underwent a preparation process that involved drying in an oven at 105°C for 24 hours and passing through a 2 mm sieve. The moist tamping method was used to prepare the samples, which is based on a technique described by Ladd (1978). This method allows for achieving a uniform distribution of density in the sample. A specific amount of soil was weighed, and distilled water was sprayed onto the samples to attain an initial moisture content of 8.1% (Sample A) and 11.8% (Sample B). The choice of 8.1% moisture for sample A was intended to explore the influence of initial compaction moisture on the extended-term variations of K_s . The samples were then covered and left for approximately 24 hours to achieve moisture balance before

146 testing. The samples were compacted in a constant head test cell with an interior diameter and
147 height of 76.2 mm and 292 mm, respectively. Compaction was carried out in layers of 12 mm. Before
148 the compaction, subsamples were taken to measure the actual moisture, particle size distribution,
149 and XRD. The final dry density of the samples was calculated from the net dry soil used and
150 compacted sample volume and listed in The soil examined in this study is river sand, commercially
151 referred to as pit sand, often employed for embankments and raised areas like pathways. The pit
152 sand used for this investigation originated from sand quarries situated in Ngahinapouri and Te
153 Kowhai, located along the Waipa River in Waikato, New Zealand, as depicted in Figure 1. For this
154 study, two samples (sample A and sample B) were taken from the same batch of pit sand provided
155 by a supplier. Sample B was used as a replication in this research.



156

157 *Figure 1- The geographical location of the Waipa River in New Zealand, with the samples originating*
158 *from sand quarries located near the Waipa riverbanks.*

159 Table 1 outlines the physical properties of the samples. Upon microscopic examination and particle
160 separation, five distinct groups are discerned (Figure 2): quartz and feldspar (approximately 60%),
161 pumice (approximately 11%), colourful particles (approximately 6%), magnetics (approximately
162 10%), and glass shards (approximately 13%). The magnetic minerals were isolated through

163 magnetic separation. X-ray diffraction (XRD) analysis was employed to assess mineral composition,
164 while the loss on ignition (LOI) method was utilised to estimate the presence of organic material in
165 the samples. The analysis of XRD data peak patterns confirms that quartz and feldspar constitute
166 the majority of minerals in the sample (Figure 3).

167 A laser diffractometer (Malvern Mastersizer 3000) was used to determine the particle size
168 distribution of the samples. For this study, the particles below $75 \mu\text{m}$ were considered as fines,
169 which aligns with the classification of ASTM for fine and coarse particles (ASTM D2487, 2020). The
170 particle size distribution results indicate that the samples are primarily sandy, with less than 10%
171 of fine materials. Particles below $5 \mu\text{m}$ were considered mobile colloidal particles (Kretzschmar et
172 al., 1999), and the percentages of these particles are also mentioned in Table 1. Based on Standard
173 Proctor tests (ASTM, 2012), the optimal compaction moisture of the samples was determined to be
174 12%.

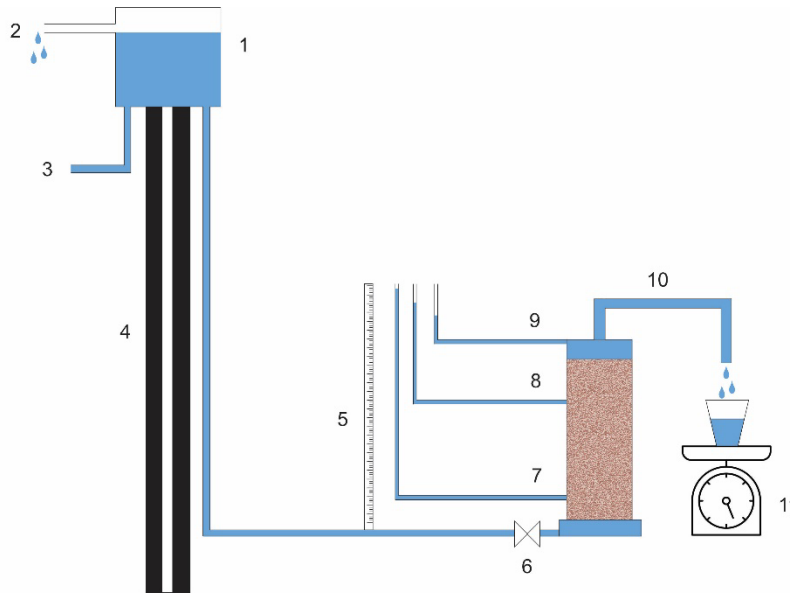
175 Table 1.

176 To achieve saturation, the samples were first connected to a vacuum pump for one hour. Distilled
177 and de-aired water was then introduced into the test cell in an upward direction, following the
178 procedure outlined in ASTM D2434-19 (ASTM, 2019), to minimise air entrapment. The samples
179 were left saturated overnight to reduce the chances of air entrapment further.

180 **3. Methods**

181 **3.1. Constant head hydraulic conductivity tests**

182 The schematic experimental apparatus used for the constant head hydraulic conductivity test is
183 shown in Figure 4. The adjustable water head tank enabled the alteration of the hydraulic head
184 during the experiment without the need to terminate the test. In addition, there were porous disks
185 with a 1 mm mesh size and a spring on top to hold the sample stable in the cell. The mesh size of the
186 porous disk was selected in a way to prevent the formation of clogging and pressure drops on the
187 disk.



188

189 *Figure 4-Schematic constant head hydraulic conductivity apparatus-(1) Water tank, (2) overflow outlet, (3)*
 190 *water supply hose, (4) adjustable level board, (5) ruler, (6) water entrance valve, (7) piezometer 1, (8)*
 191 *piezometer 2, (9) piezometer 3, (10) water outlet, (11) scale for measuring the discharge*

192 The water flow and head gradient were measured at least thrice daily. The collection of effluent in a
 193 bucket was carried out for each flow measurement, and the duration of the effluent collection was
 194 recorded. Subsequently, the discharge was calculated by dividing the weight of the collected
 195 effluent by the collection duration.

196 The tests were conducted in a back-and-forth pattern with water heads ranging from 963 mm to
 197 1765 mm, with increments and decrements of approximately 200 mm. The hydraulic head began at
 198 a minimum of 963 mm and was incrementally increased by around 200 mm until it reached a
 199 maximum of 1765 mm. Subsequently, the head followed the same pattern of decrease in sequential
 200 steps. The testing period has lasted for approximately 53 days. Detailed information on the test
 201 numbers, hydraulic heads, and durations can be found in **Error! Reference source not found.**

202 *Table 2- Hydraulic Head and Durations of Constant Head Tests on Samples A and B*

Test Number	1	2	3	4	5	6	7	8	9	10
Hydraulic head (mm)	963	1163	1365	1558	1765	1558	1365	1163	963	Varies
Sample A Duration (days)	5	6	6	6	5	3	7	6	7	1

Sample B Duration (days)	5	5	5	5	5	5	5	5	31	N/A
-----------------------------	---	---	---	---	---	---	---	---	----	-----

203

204 During the testing process, the pressure and discharge readings were recorded simultaneously by
 205 three piezometers. As depicted in Figure 4, the pressure inside the sample was measured by two
 206 piezometers located at points 7 and 8, while the piezometer at point 9 measured the water head at
 207 the discharge point on the opposite end of the cell.

208 After completing test 9 on sample *A*, the water flow was not stopped, and a moderately rapid
 209 constant head test was conducted using the same hydraulic heads as tests 1 to 9. This test,
 210 designated as "Test 10", lasted approximately 16 hours, with each constant head being run for
 211 about 2 hours. The purpose of Test 10 was to observe any changes in *Ks* under a shorter duration
 212 and to determine if the *Ks* during the head-increasing stage were similar to the reciprocal *Ks* during
 213 the head-decreasing stage.

214 In the case of sample *B*, test 9 was allowed to run for 31 days at the minimum head (963 *mm*) after
 215 an increasing trend in the *Ks* of the sample was observed from day 53 onwards. The purpose was to
 216 determine how long the *Ks* would continue to change and whether it would return to a value similar
 217 to the beginning of the test.

218 In order to examine changes in soil properties during the test, the samples were recovered from the
 219 hydraulic conductivity cell. After extraction, the samples were divided into three sections: bottom,
 220 middle, and top. Subsequently, particle size distribution and specific gravity measurements were
 221 conducted on these sub-samples to assess any variations resulting from the test.

222 4. Results

223 4.1. Long-term *Ks* Tests

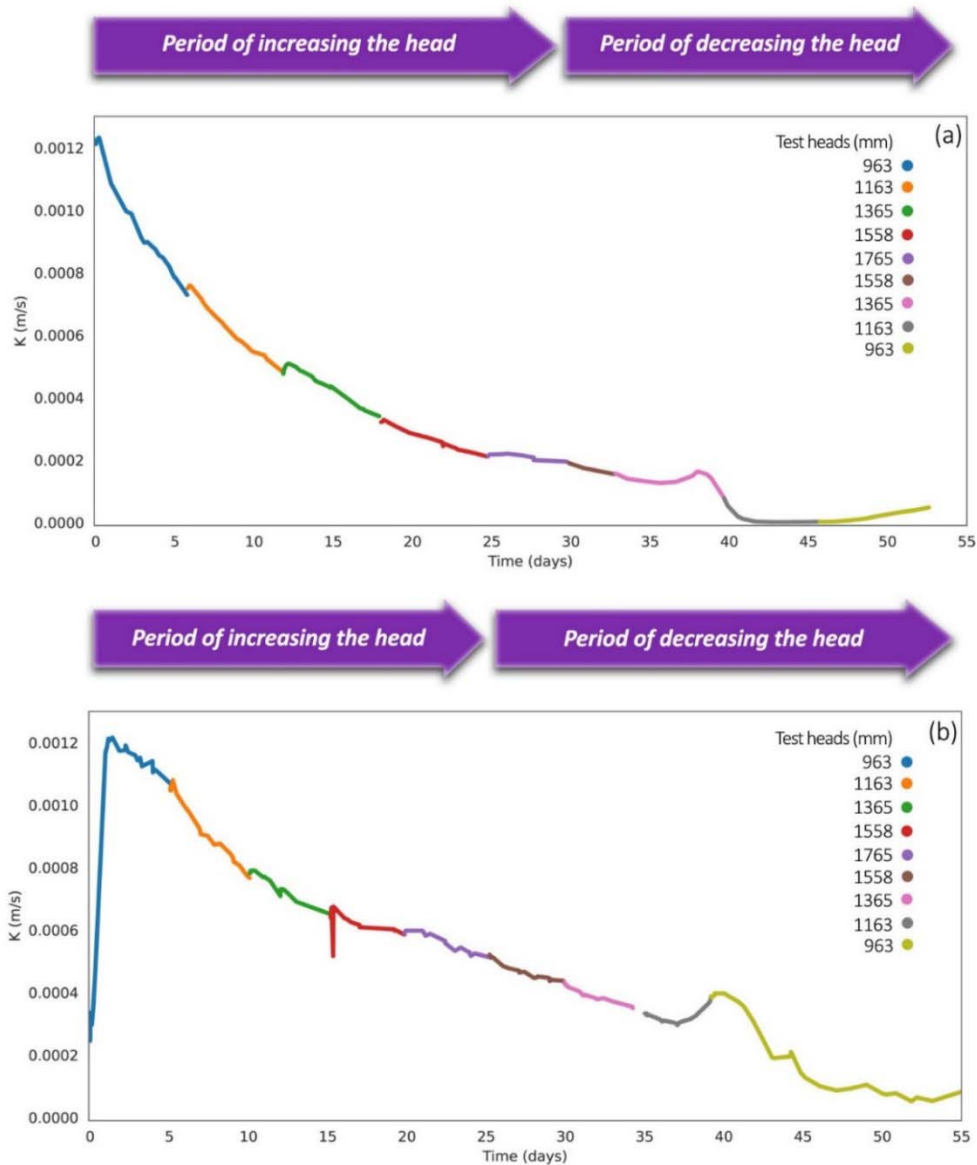
224 The long-term change in *Ks* calculated for both samples is illustrated in Figure 5. The *Ks* values of
 225 the samples showed a general decline throughout the tests, as shown in Figure 5, except for three
 226 brief periods. These periods occurred between days 36 to 38 for sample *A* and between days 0 to 1
 227 and 37 to 40 for sample *B*.

228 Furthermore, there are two distinct periods of a noticeable increase in *Ks* in both samples, which
 229 coincide closely in timing, specifically between days 35 and 40. In sample *A*, the increase in *Ks* starts
 230 at 1365 *mm* head and ends at the same head in Figure 5a. However, in sample *B*, *Ks* starts

231 increasing at 1163 *mm* head and starts decreasing again at 963 *mm* head in Figure 5b. There is no
232 clear answer to why *K_s* increases in the mentioned periods in the samples. At the end of the tests,
233 the final *K_s* values for samples *A* and *B* were 96% and 91% lower than their maximum, respectively.

234 The initial moisture levels (8.1% for sample *A* and 11.8% for sample *B*) appear to have had limited
235 influence on the extended-term variation of *K_s*. However, they might have played a role in the initial
236 stages of permeation. Figure 5 illustrates that sample *A* achieved its maximum *K_s* within the first
237 few hours of commencing the test. In contrast, sample *B* took approximately two days to reach its
238 peak *K_s*.

239 Also, throughout the head increase cycle, a notable pattern emerges: at the onset of each hydraulic
240 head increment, there is a marginal uptick in *K_s*, which is subsequently followed by a sustained
241 decrease. This minor elevation in *K_s* can be attributed to the abrupt rise in the hydraulic head.

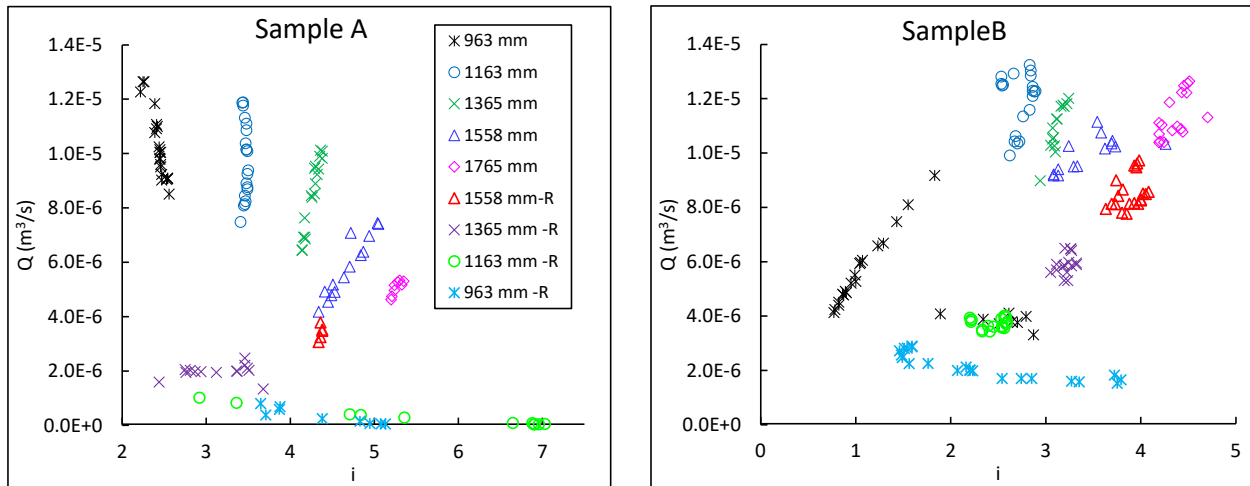


242

243 *Figure 5- Changes of Ks over time for samples A (a) & B (b)- the generally reducing trend in Ks is*
 244 *noticeable in both samples*

245 4.2. Flow-head gradient relationship

246 In the hypothetical scenario, where the samples remained unchanged throughout the tests, Darcy's
 247 law would anticipate the clustering of all data points at each hydraulic head increment around a
 248 single point, forming a unified line. Figure 6 illustrates the relationship between flow rate (Q) and
 249 hydraulic head gradient (i) within samples A and B across varying hydraulic head levels. The
 250 symbol "R" signifies the period characterised by a decreasing head. The scatterplots demonstrate
 251 the absence of a straightforward linear correlation between Q and i.



252

253 *Figure 6: Scatterplots exploring the correlation between head gradient and flow rate in samples A*
 254 *and B with different hydraulic head levels. The symbol "R" signifies the period characterised by a*
 255 *decreasing hydraulic head.*

256 In the case of sample A, during test phases 1 to 4, wherein the head is incrementally raised every 5
 257 or 6 days from 963 to 1765 mm, a decrease in flow accompanied by an increase in head gradient
 258 becomes evident. Interestingly, even within each step, the scatterplot does not exhibit the expected
 259 convergence around a single point, as outlined by Darcy's law. This suggests a dynamic nature of
 260 the sample during this period, with the hydraulic conductivity undergoing continuous changes.
 261 However, test 5, characterised by the maximum head of 1765 mm and a 5-day observation period,
 262 showcases a remarkable consistency in both head gradient and flow rate, implying a phase of
 263 stability.

264 Furthermore, as the head is reduced to 1558mm, this stability persists, with the scatterplot points
 265 clustering around a single location and both flow rate and head gradient diminishing. On the
 266 contrary, during tests 7 to 9, where the head drops from 1365 to 963 mm, the scatterplot points
 267 display unpredictable distribution, deviating significantly from the expectations of Darcy's law. This
 268 observation indicates a departure from the anticipated behaviour of the sample.

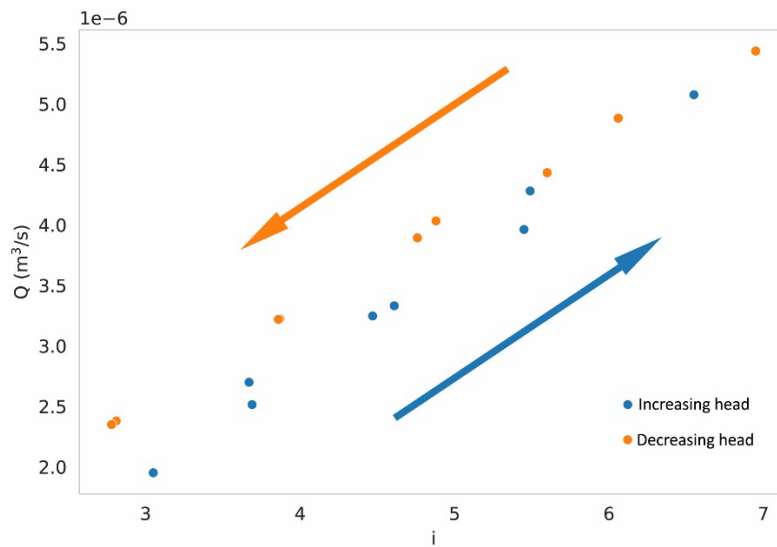
269 In sample B, the initial test with a head of 963 mm shows an unexpected trend where both the head
 270 gradient and flow rate increase, deviating from the expected convergence around a single point. As
 271 we move through tests 2 to 4, involving a hydraulic head increase from 1163 to 1558 mm, a distinct
 272 behaviour emerges: despite the elevated hydraulic head, the head gradient rises while the flow rate
 273 unexpectedly drops. This pattern suggests a shift in the hydraulic properties of the samples.

274 Nevertheless, when the hydraulic head is raised to 1765 mm and subsequently reduced to 1163
275 mm over four 5-day intervals, the sample aligns somewhat better with the predictions of Darcy's
276 law. Data points cluster more closely around a central location, and the flow rate responds to
277 changes in the hydraulic head. However, variations still exist at each step. In contrast, at the lowest
278 head level of 963 mm, there's an increase in head gradient while the flow rate remains stable.

279 4.3. Sample A behaviour in a relatively short-duration test

280 Test 10 was carried out to ensure that the variations in K_s and Q - i relation are not noticeable in the
281 short term. In this test, the sample exhibited a distinct behaviour compared to the other tests. The
282 test involved subjecting the sample to a cycle of increasing and decreasing hydraulic heads, similar
283 to the previous tests, but for a shorter period of approximately 16 hours.

284 Interestingly, this relatively quick test demonstrated a strong linear correlation between the water
285 flux and the gradient within the sample, as expected by the Darcy law. The hydraulic conductivity
286 was determined to be $7 \times 10^{-7} \text{ m/s}$ during the increasing stage of the test head and $8 \times 10^{-7} \text{ m/s}$ during
287 the decreasing stage. The correlation between Q and i is illustrated in Figure 7. Contrary to Figure 6,
288 a notably stronger correlation between Q and i can be observed.



289

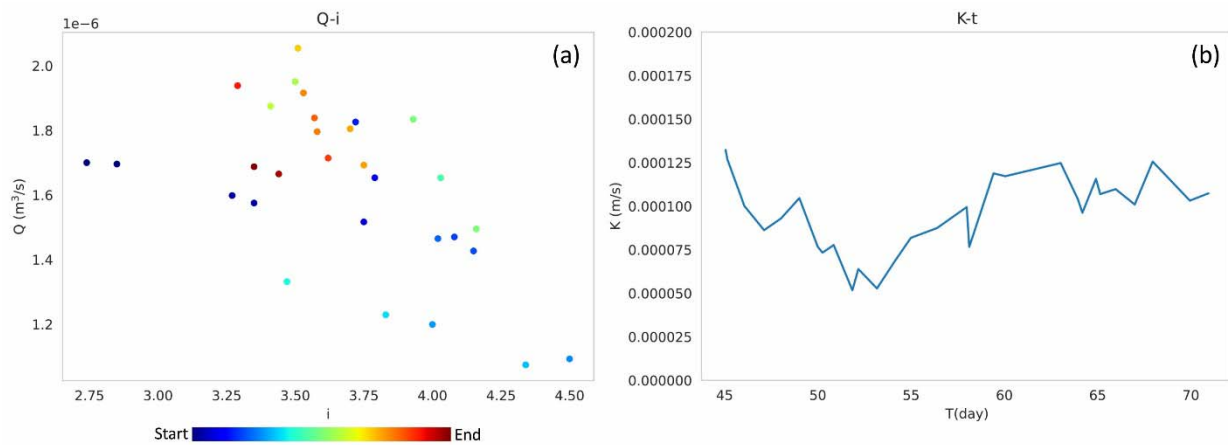
290 *Figure 7- The relationship between Q and i in test 10 for sample A, where the gradients are varied. The*
291 *blue and orange arrows represent the periods of increasing and decreasing test heads, respectively.*

292 4.4. Extending the sample B in the minimum constant head for 31 days

293 Test B has been extended for an additional 31-day period under the minimum head condition (963
294 mm). This extension aims to investigate whether hydraulic conductivity comes into stability
295 without any disruptions.

296 Figure 8(a) depicts the correlation between flow rate and head gradient during this period. The $Q-i$
297 correlation exhibits unpredictable fluctuations in both hydraulic gradient and flow rate, mirroring
298 the patterns observed in the preceding 45 days, as shown in Figure 6.

299 The temporal evolution of K_s is visually outlined in Figure 8(b). The variability of K_s spans from
300 1.25×10^{-4} m/s to 0.5×10^{-4} m/s, centring around a median value of 1.0×10^{-4} mm. In summary, the
301 continuation of the testing procedure with a consistent hydraulic head maintained over the course
302 of 31 days does not result in the stabilisation of the hydraulic conductivity of the sample. The K_s
303 values persistently oscillate within a range of +33% and -46% around the median value, thereby
304 underscoring the absence of stability in the system. However, a decreasing trend is absent in
305 contrast to previous observation periods.



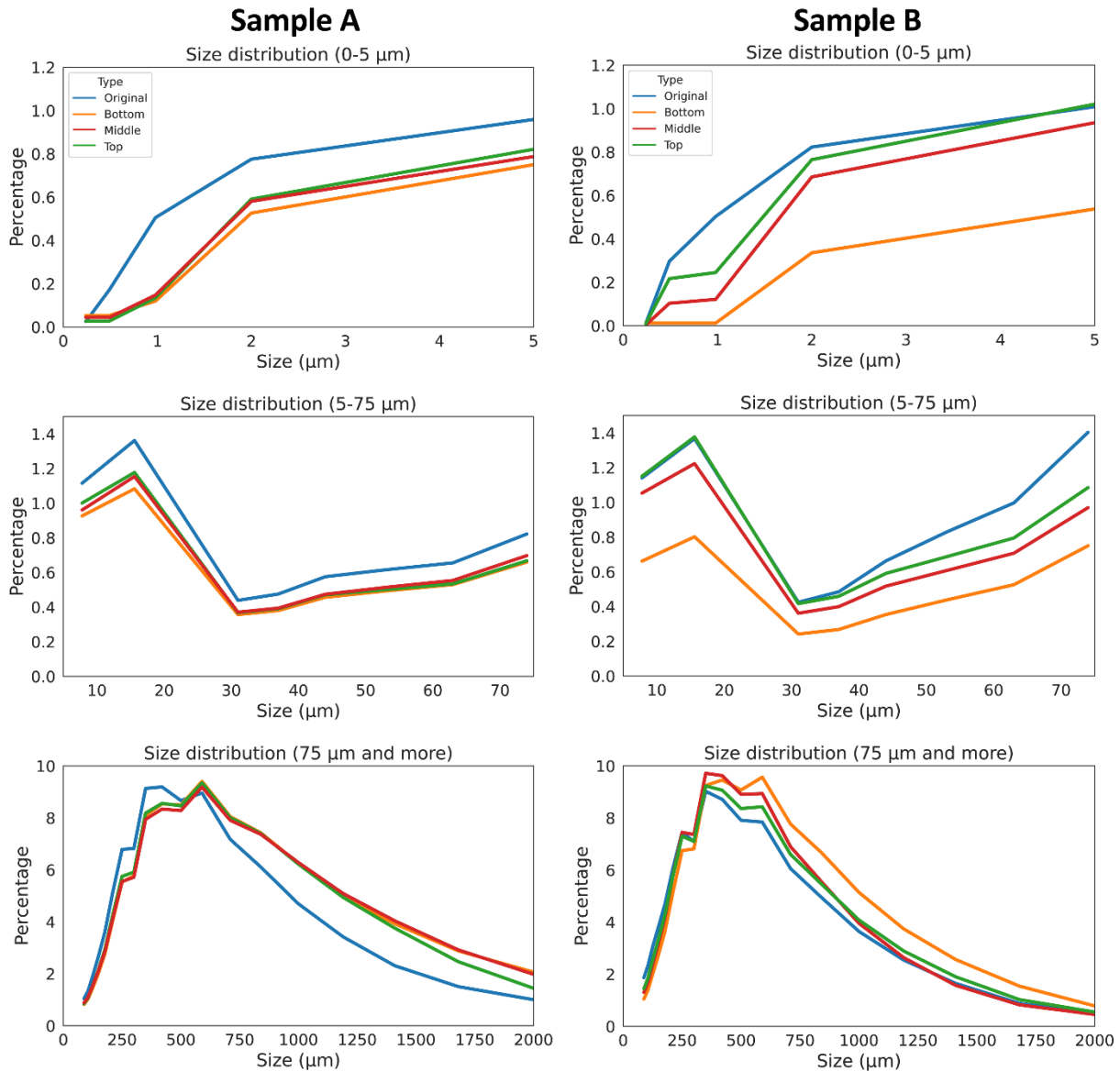
306

307 *Figure 8- (a) The relationship between Q and i for sample B during an extended period (31 days) of*
308 *running test 9 at the minimum hydraulic head. The colour spectrum and arrows depict the temporal*
309 *sequence of the measurements. (b) The changes in K_s over time for sample B during the same 31-day*
310 *duration of test 9 at the minimum hydraulic head.*

311 4.5. Comparison of soil properties before and after the tests

312 In order to assess the influence of the constant head test on soil properties, particle size
313 distribution (PSD) and specific gravity (GS) measurements were performed on both the original soil
314 samples and different sections of the soil after the test. This investigation aimed to understand how
315 the test influenced the PSD and density characteristics of the soil samples.

316 Figure 9 shows the PSD of the sample's top, middle, and bottom sections and the original
 317 sample prior to the test. Additionally, Table 3 compares the total particles below and above 75 μm
 318 for reference. The results in Table 3 indicate that the sample's total percentage of fine particles
 319 decreased after the tests. Approximately 2% of fine particles in sample A and 1% in sample B were
 320 washed away during the long-term tests. It is noteworthy that samples A and B contained less than
 321 9% of fine particles (below 75 μm).



322

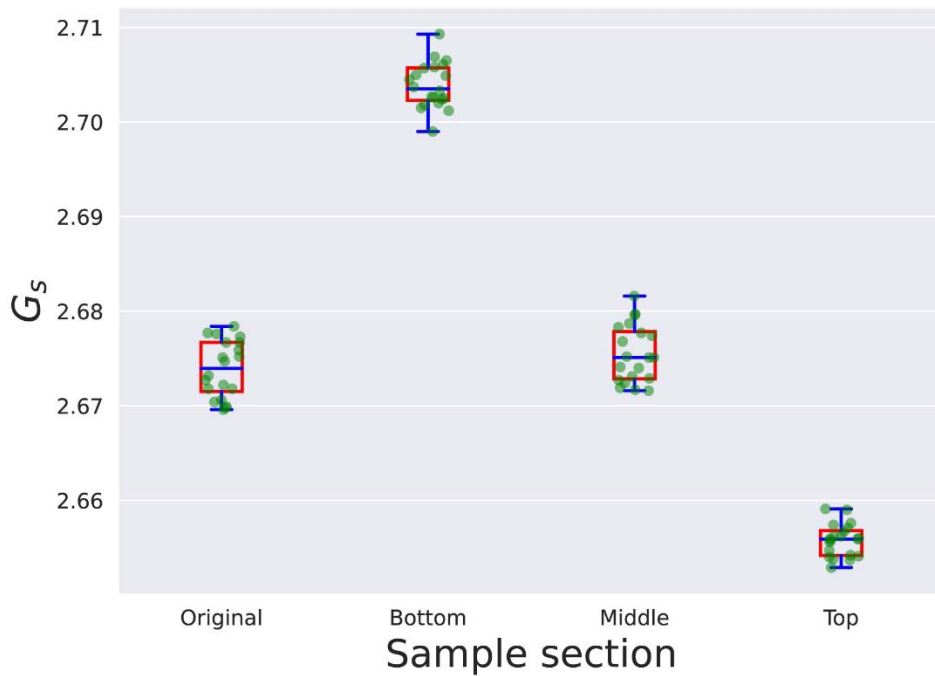
323 *Figure 9- Particle size analysis of the samples (comparison of the samples before tests and after tests,*
 324 *divided by sub-samples of different sections)*

325

326
327

Table 3- Comparison of total percentage of particles below and above 64 μm before and after tests divided by different sections in the sample

Totals (%)	Sample A				Sample B			
	Original	Bottom	Middle	Top	Original	Bottom	Middle	Top
Below 75 μm	7.37	5.09	5.41	5.74	8.42	4.06	6.68	7.63
Above 75 μm	92.61	94.91	94.59	94.26	91.58	95.94	93.32	92.37



328

329 Figure 10- Specific gravity of sample A before and after test divided by sub-samples of different
330 sections

331 Figure 9 and Table 3 show that the percentage of fine particles below 75 μm is highest at the top
332 section of the samples, followed by the middle and bottom sections. While the difference in the
333 percentage of fine particles among different sections is minor for sample A (less than 1%), it is
334 higher for sample B (around 3%).

335 Gs measurements are presented as a box plot in Figure 10. The box plots illustrate notable changes
336 in the specific gravity of the sample in comparison to the original sample. The lowest Gs is found at

337 the bottom section of sample A, while the highest G_s is observed at the top section, with a slight
338 increase in the middle section.

339 **5. Discussion**

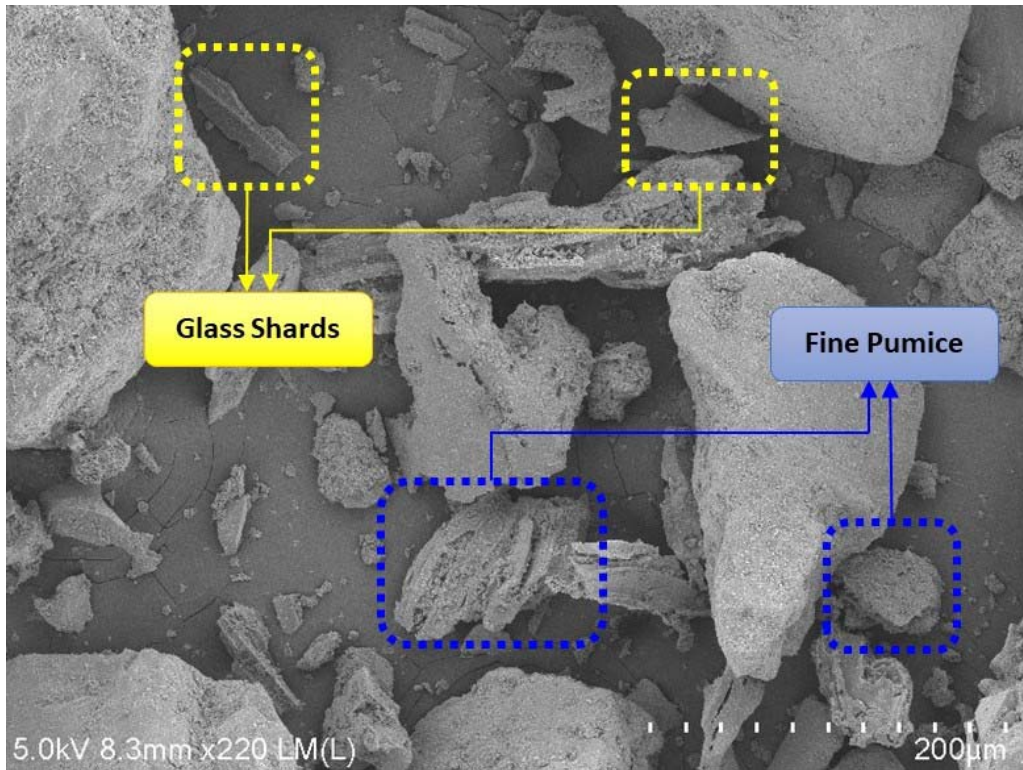
340 Examining soil properties in the original sample before and after the constant head test reveals
341 notable alterations in the soil characteristics. These changes directly impact the hydraulic
342 conductivity, highlighting the direct influence of the test on soil properties and subsequent
343 hydraulic behaviour. For example, Figure 5(a & b) demonstrates a prevailing long-term decreasing
344 trend in K_s . However, it is important to note that there are also intermittent shorter periods where
345 K_s show an increase. This observation highlights the dynamic nature of the system, wherein both
346 long-term trends and shorter-term fluctuations in hydraulic conductivity are evident.

347 The K_s tests on the coarse particles (sandy samples with less than 10% fines) are generally short
348 because the variation of K_s is very marginal during the first few hours of the tests. For example, in
349 sample A, the change of K_s during the first 5 hours from starting the test was only 2%, which is
350 negligible. However, after five days, the K_s dropped by 40%, and at the end of the test, the K_s
351 dropped by around 96% from the beginning of the test.

352 Figure 6 clearly represents the dynamic nature of the samples' hydraulic gradient and pore
353 pressure. These parameters undergo continuous fluctuations without exhibiting a consistent
354 decreasing or increasing pattern. Even extending the test for a longer period (Figure 8 (a) and (b))
355 does not create a stable gradient in the sample. Therefore, it can be inferred that the connectivity of
356 the drainable pores is constantly changing. This observation underscores the complex behaviour of
357 the hydraulic system within the samples, emphasising the need to consider the temporal variations
358 in pore pressure when analysing the overall hydraulic response.

359 The variations in the hydraulic gradient and discharge relation, and hence hydraulic conductivity in
360 the samples, can be attributed to several factors. According to the ASTM standard (ASTM, 2015), air
361 entrapment can potentially reduce hydraulic conductivity. In this research, a primary focus was
362 minimising air entrapment within the sample during saturation. As a result, no visible evidence of
363 air entrapment was observed during the test. The transparent acrylic test cell facilitated direct
364 observation of the sample particles throughout the experiment. The absence of any noticeable
365 formation of air bubbles among the particles from the sides of the samples suggests that air
366 entrapment is unlikely to contribute to the observed reduction in K_s in our study.

367 Another factor that can affect the continuous reduction of K_s is the blockage of drainable pores with
368 fine particles (Jeong et al., 2018b), which restricts the flow of water and leads to a decrease in the
369 K_s . Particle size distribution of the samples (Figure 9) shows that the fine particles in all sections
370 have decreased compared to the original sample prior to the test. Furthermore, there is a decrease
371 in G_s in the top section and an increase in the bottom section (Figure 10). It can be concluded that
372 mobile low-density fine particles (such as fine pumice) have displaced from the bottom of the
373 sample to the top. Another reason for the reduction in the K_s can be related to the continuous
374 blockage of the drainable pores with fine particles with rough surfaces (such as glass shards) or the
375 simultaneous impact of blockage by glass shards and mobilisation and blockage by low-density
376 particles. The SEM image of the sample in Figure 11 shows a noticeable amount of glass shards and
377 pumice in the small section of the sample. Continuous mobilisation or re-deposition of these
378 particles can change the connection of the drainable pores and reduce K_s .



379

380 *Figure 11- 220x magnification of the sample using SEM providing a closer view of the fine particles in*
381 *the sample*

382 The ASTM standard for granular soils (ASTM, 2019a) explains the procedure of estimating the K_s
383 without mentioning the period of carrying out each test. The long-term K_s results in Figure 6 show
384 a noticeable drop in the K_s , and if the test is terminated in a few hours, the resulting K_s will be 96%

385 higher than the final one. Similar results were reported by (Du et al., 2018; Vanderzalm et al., 2020),
386 when they permeated the sample with a solution containing *Fe (III)* or water with suspended solids.
387 In our research, there was no *Fe (III)* contamination source, and the water used was drinking water
388 from a tap. Figure 7 demonstrates a robust linear relationship between Q and i during the
389 increasing and decreasing head phases during short-term testing. However, when comparing this
390 figure to the long-term tests illustrated in Figure 6, it becomes evident that the Q - i relationship
391 varies over time.

392 The long-term variability of hydraulic conductivity holds significant importance for systems
393 enduring extended saturation periods. For instance, artificial soakage basins and soak pits are
394 frequently recommended in the context of stormwater management in new urban developments
395 (Shaver, 2020). These systems gather runoff from urban areas and gradually infiltrate the water
396 into the ground. A crucial factor in designing these soakage systems is the saturated hydraulic
397 conductivity. However, it's important to note that the testing duration commonly used to assess the
398 K_s rate is often short and may not accurately represent the long-term behaviour of hydraulic
399 conductivity. Consequently, it's wise to account for the long-term variation of K_s when reporting K_s
400 values for applications involving soil saturation, such as soakage basins or drainage pipes. This
401 precaution is essential as overestimation could lead to erroneous calculations.

402 **6. Conclusion**

403 This study provides valuable insights into the variation of hydraulic conductivity in sandy samples
404 through a long-term constant head experiment. The results demonstrate a significant reduction in
405 K_s , primarily due to physical clogging caused by fines and pumice particles. The increased
406 concentration of pumice particles in the top section indicates their mobility and potential blockage
407 of drainable pore sections, affecting K_s . These changes were not observed in short-term tests,
408 highlighting the importance of longer-term investigations. The findings stress the need for
409 extended constant head tests to accurately assess and report K_s in sandy samples, enhancing our
410 understanding of their hydraulic behaviour. These findings have practical implications in various
411 geotechnical engineering applications, such as groundwater remediation, landfill design,
412 geotechnical stability analysis, and drainage system design.

413 **7. Acknowledgment**

414 This research was supported by the University of Waikato Doctoral Scholarship.

415 8. Data Availability Statement

416 All data used and generated by this study, including hydraulic head and flow measurements, can be
417 found in [PDI-36052](#).

418 9. References

- 419 ASTM. (2019). Standard Test Method for Permeability of Granular Soils (Constant Head)
420 (D2434-19). *ASTM International, West Conshohocken, PA*. <https://doi.org/10.1520/D2434-19>
- 421 ASTM D2434-19. (2019). Standard Test Method for Permeability of Granular Soils (Constant
422 Head). *ASTM International, West Conshohocken, PA*. <https://doi.org/10.1520/D2434-19>
- 423 ASTM D2487. (2020). Standard Practice for Classification of Soils for Engineering Purposes
424 (Unified Soil Classification System). *ASTM*.
- 425 ASTM D5856-15. (2015). Standard Test Method for Measurement of Hydraulic Conductivity of
426 Porous Material Using a Rigid-Wall, Compaction-Mold Permeameter. *ASTM International, West
427 Conshohocken, PA*.
- 428 Ben-Hur, M., Yolcu, G., Uysal, H., Lado, M., & Paz, A. (2009). Soil structure changes: Aggregate
429 size and soil texture effects on hydraulic conductivity under different saline and sodic
430 conditions. *Australian Journal of Soil Research*. <https://doi.org/10.1071/SR09009>
- 431 Boadu, F. K. (2000). Hydraulic Conductivity of Soils from Grain-Size Distribution: New Models.
432 *Journal of Geotechnical and Geoenvironmental Engineering*, 126(8), 739–746.
433 [https://doi.org/10.1061/\(ASCE\)1090-0241\(2000\)126:8\(739\)](https://doi.org/10.1061/(ASCE)1090-0241(2000)126:8(739))
- 434 Chaneva, J., Kluger, M. O., Moon, V. G., Lowe, D. J., & Orense, R. P. (2023). Monotonic and cyclic
435 undrained behaviour and liquefaction resistance of pumiceous, non-plastic sandy silt. *Soil
436 Dynamics and Earthquake Engineering*, 168, 107825.
437 <https://doi.org/10.1016/j.soildyn.2023.107825>
- 438 Cihan, A., Petrusak, R., Bhuvankar, P., Alumbaugh, D., Trautz, R., & Birkholzer, J. T. (2022).
439 Permeability Decline by Clay Fines Migration around a Low-Salinity Fluid Injection Well.
440 *Groundwater*, 60(1), 87–98. <https://doi.org/10.1111/gwat.13127>
- 441 Du, X., Wang, Z., & Ye, X. (2013). Potential Clogging and Dissolution Effects During Artificial
442 Recharge of Groundwater Using Potable Water. *Water Resources Management*, 27(10), 3573–
443 3583. <https://doi.org/10.1007/S11269-013-0365-5/FIGURES/13>

444 Du, X., Zhang, H., Ye, X., & Lu, Y. (2018). Flow Velocity Effects on Fe(III) Clogging during
445 Managed Aquifer Recharge Using Urban Storm Water. *Water* 2018, Vol. 10, Page 358, 10(4),
446 358. <https://doi.org/10.3390/W10040358>

447 Fang, Y., Kong, L., Zhang, P., Zhang, L., Zhao, H., Xiang, X., Cheng, S., Zhang, H., Ju, F., & Li, L.
448 (2022). Fifteen-year analysis of constructed wetland clogging: A critical review. *Journal of*
449 *Cleaner Production*, 365, 132755.
450 <https://doi.org/https://doi.org/10.1016/j.jclepro.2022.132755>

451 Francisca, F. M., & Glatstein, D. A. (2010). Long term hydraulic conductivity of compacted soils
452 permeated with landfill leachate. *Applied Clay Science*.
453 <https://doi.org/10.1016/j.clay.2010.05.003>

454 Hwang, H. T., Jeon, S. W., Suleiman, A. A., & Lee, K. K. (2017). Comparison of saturated
455 hydraulic conductivity estimated by three different methods. *Water (Switzerland)*.
456 <https://doi.org/10.3390/w9120942>

457 Jeong, H. Y., Jun, S. C., Cheon, J. Y., & Park, M. (2018a). A review on clogging mechanisms and
458 managements in aquifer storage and recovery (ASR) applications. *Geosciences Journal*, 22(4),
459 667–679. <https://doi.org/10.1007/S12303-017-0073-X/METRICS>

460 Jeong, H. Y., Jun, S.-C., Cheon, J.-Y., & Park, M. (2018b). A review on clogging mechanisms and
461 managements in aquifer storage and recovery (ASR) applications. *Geosciences Journal*, 22(4),
462 667–679. <https://doi.org/10.1007/s12303-017-0073-x>

463 Jo, H. Y., Benson, C. H., Shackelford, C. D., Lee, J.-M., & Edil, T. B. (2005). Long-Term Hydraulic
464 Conductivity of a Geosynthetic Clay Liner Permeated with Inorganic Salt Solutions. *Journal of*
465 *Geotechnical and Geoenvironmental Engineering*. [https://doi.org/10.1061/\(asce\)1090-](https://doi.org/10.1061/(asce)1090-0241(2005)131:4(405))
466 [0241\(2005\)131:4\(405\)](https://doi.org/10.1061/(asce)1090-0241(2005)131:4(405))

467 Kikkawa, N., Orense, R. P., & Pender, M. J. (2013). Observations on microstructure of pumice
468 particles using computed tomography. *Canadian Geotechnical Journal*, 50(11), 1109–1117.
469 <https://doi.org/10.1139/cgj-2012-0365>

470 Konikow, L. F., August, L. L., & Voss, C. I. (2001). Effects of Clay Dispersion on Aquifer Storage
471 and Recovery in Coastal Aquifers. *Transport in Porous Media*, 43(1), 45–64.
472 <https://doi.org/10.1023/A:1010613525547>

473 Kretzschmar, R., Borkovec, M., Grolimund, D., & Elimelech, M. (1999). *Mobile Subsurface*
474 *Colloids and Their Role in Contaminant Transport* (pp. 121–193).
475 [https://doi.org/10.1016/S0065-2113\(08\)60427-7](https://doi.org/10.1016/S0065-2113(08)60427-7)

476 Ladd, R. (1978). Preparing Test Specimens Using Undercompaction. *Geotechnical Testing*
477 *Journal*, 1(1), 16. <https://doi.org/10.1520/GTJ10364J>

478 Li, K., Chen, Y., Ye, W., & Wang, Q. (2023). Modelling the evolution of dual-pore structure for
479 compacted clays along hydro-mechanical paths. *Computers and Geotechnics*, 157, 105308.
480 <https://doi.org/https://doi.org/10.1016/j.compgeo.2023.105308>

481 Liu, L., Orense, R., & Pender, M. (2015). Crushing-induced liquefaction characteristics of
482 pumice sand. *Proc., Australia-New Zealand Conference on Geomechanics*.

483 Liu, Y., & Liu, J. (2020). The BioChemical Clogging of Landfill Leachate Collection System: Based
484 on Laboratory Studies. *International Journal of Environmental Research and Public Health*,
485 17(7), 2299. <https://doi.org/10.3390/ijerph17072299>

486 Lu, H., Wang, C., Li, D., Li, J., & Wan, Y. (2020). Permeability, Pore, and Structural Parameters of
487 Undisturbed Silty Clay Presented in Landfill Leachate. *Water, Air, & Soil Pollution*, 231(5), 190.
488 <https://doi.org/10.1007/s11270-020-04568-0>

489 Mays, D. C., & Hunt, J. R. (2005). Hydrodynamic Aspects of Particle Clogging in Porous Media.
490 *Environmental Science & Technology*, 39(2), 577–584. <https://doi.org/10.1021/es049367k>

491 Mohan, K. K., Vaidya, R. N., Reed, M. G., & Fogler, H. S. (1993). Water sensitivity of sandstones
492 containing swelling and non-swelling clays. *Colloids and Surfaces A: Physicochemical and*
493 *Engineering Aspects*, 73, 237–254. [https://doi.org/10.1016/0927-7757\(93\)80019-B](https://doi.org/10.1016/0927-7757(93)80019-B)

494 Montoro, M. A., & Francisca, F. M. (2010). Soil Permeability Controlled by Particle-Fluid
495 Interaction. *Geotechnical and Geological Engineering*. [https://doi.org/10.1007/s10706-010-](https://doi.org/10.1007/s10706-010-9348-y)
496 9348-y

497 Shaver, E. (2020). Waikato stormwater management guideline.

498 Siriwardene, N., Deletic, A., & Fletcher, T. (2007). Clogging of stormwater gravel infiltration
499 systems and filters: Insights from a laboratory study. *Water Research*, 41(7), 1433–1440.
500 <https://doi.org/10.1016/j.watres.2006.12.040>

501 Song, W., Liu, X., Zheng, T., & Yang, J. (2020). A review of recharge and clogging in sandstone
502 aquifer. *Geothermics*, 87, 101857. <https://doi.org/10.1016/j.geothermics.2020.101857>

503 Suleiman, A. A., & Ritchie, J. T. (2001). Estimating saturated hydraulic conductivity from soil
504 porosity. *Transactions of the American Society of Agricultural Engineers*.
505 <https://doi.org/10.13031/2013.4683>

506 Torkzaban, S., Bradford, S. A., Vanderzalm, J. L., Patterson, B. M., Harris, B., & Prommer, H.
507 (2015). Colloid release and clogging in porous media: Effects of solution ionic strength and
508 flow velocity. *Journal of Contaminant Hydrology*, 181, 161–171.
509 <https://doi.org/10.1016/j.jconhyd.2015.06.005>

510 Touze-Foltz, N., Duquennoi, C., & Gaget, E. (2006). Hydraulic and mechanical behavior of GCLs
511 in contact with leachate as part of a composite liner. *Geotextiles and Geomembranes*, 24(3),
512 188–197. <https://doi.org/https://doi.org/10.1016/j.geotexmem.2006.01.004>

513 Valencia-González, Y., Quintero-Ramírez, A., & Lara-Valencia, L. A. (2022). A laboratory
514 methodology for predicting variations in the geotechnical parameters of soil exposed to solid
515 waste leachates in the field. *Results in Engineering*, 14, 100398.
516 <https://doi.org/https://doi.org/10.1016/j.rineng.2022.100398>

517 Vanderzalm, J. L., Page, D. W., Barry, K. E., & Gonzalez, D. (2020). Evaluating Treatment
518 Requirements for Recycled Water to Manage Well Clogging during Aquifer Storage and
519 Recovery: A Case Study in the Werribee Formation, Australia. *Water 2020*, Vol. 12, Page 2575,
520 12(9), 2575. <https://doi.org/10.3390/W12092575>

521 VanGulck, J. F., & Rowe, R. K. (2004). Evolution of clog formation with time in columns
522 permeated with synthetic landfill leachate. *Journal of Contaminant Hydrology*.
523 <https://doi.org/10.1016/j.jconhyd.2004.06.001>

524 Wang, W., Dong, L., Zhai, T., Wang, W., Wu, H., Kong, F., Cui, Y., & Wang, S. (2023). Bio-clogging
525 mitigation in constructed wetland using microbial fuel cells with novel hybrid air-
526 photocathode. *Science of The Total Environment*, 881, 163423.
527 <https://doi.org/https://doi.org/10.1016/j.scitotenv.2023.163423>

528 Wang, Y., Yu, M., Bo, Z., Bedrikovetsky, P., & Le-Hussain, F. (2021). Effect of temperature on
529 mineral reactions and fines migration during low-salinity water injection into Berea

530 sandstone. *Journal of Petroleum Science and Engineering*, 202, 108482.

531 <https://doi.org/10.1016/j.petrol.2021.108482>

532 Wang, Z., Du, X., Yang, Y., & Ye, X. (2012). Surface clogging process modeling of suspended
533 solids during urban stormwater aquifer recharge. *Journal of Environmental Sciences*, 24(8),
534 1418–1424. [https://doi.org/10.1016/S1001-0742\(11\)60961-3](https://doi.org/10.1016/S1001-0742(11)60961-3)

535 Ye, X., Cui, R., Du, X., Ma, S., Zhao, J., Lu, Y., & Wan, Y. (2019). Mechanism of Suspended Kaolinite
536 Particle Clogging in Porous Media During Managed Aquifer Recharge. *Groundwater*, 57(5),
537 764–771. <https://doi.org/10.1111/gwat.12872>

538